A theoretical analysis of steady three-dimensional flow and heat transfer of Power-Law nanofluid over a stretchable rotating disk filled with gyrotactic microorganisms

Usman; Lin, Ping; Ghaffari, Abuzar; Mustafa, Irfan

Published in:
Physica Scripta

DOI:
10.1088/1402-4896/abc647

Publication date:
2021

Document Version
Peer reviewed version

A theoretical analysis of steady three-dimensional flow and heat transfer of Power-Law nanofluid over a stretchable rotating disk filled with gyrotactic microorganisms

Usman1*, Ping Lin2†, Abuzar Ghaffari[3], Irfan Mustafa[4]

[1]Beijing Key Laboratory for Magneto-Photoelectrical Composite and Interface Science, Department of Applied Mathematics, School of Mathematics and Physics, University of Science and Technology Beijing, Beijing 100083, China

[2]Division of Mathematics, University of Dundee, Dundee, DD1 4HN, Scotland, United Kingdom

[3]Department of Mathematics, University of Education, Lahore (Attock Campus 43600), Pakistan

[4]Department of Mathematics, Allama Iqbal Open University, H-8, Islamabad 44000, Pakistan

E-mail: **usman.malik.ms@gmail.com**, **p.lin@dundee.ac.uk**

Received xxxxxx
Accepted for publication xxxxxx
Published xxxxxx

Abstract

The current research study investigates the steady three-dimensional flow and heat transfer of a power-law nanofluid in the presence of the uniformly applied magnetic field and nonlinear thermal radiation over the stretchable rotating disk filled with gyrotactic microorganisms. The physically modeled partial differential equations (PDEs) are lessened to combined nonlinear ordinary differential equations (ODEs) with appropriate transformation. The influence of several types of pertinent parameters upon the distributions of velocity, temperature, the concentration of nanoparticles, and microorganisms are analyzed graphically by solving the ODEs with a well-known shooting method. The tabular comparison is provided for the verification between the present results with those in the literature. Also, the physical quantities of interest are calculated, and the effects are scrutinized. Furthermore, it is noticed that the emerging parameters have produced a significant influence upon the velocity components, temperature, concentration of nanoparticles, and motile density of microorganisms.

Keywords: Power-law nanofluid, nonlinear thermal radiation, MHD boundary layer flow, gyrotactic microorganisms, stretchable rotating disk.

* Corresponding author: usman.malik.ms@gmail.com / (Usman)
† Corresponding author: p.lin@dundee.ac.uk/ (Ping Lin)

1. Introduction

Fluid flow phenomenon because of the disk rotation is a dynamic area of research and of particular interest, which leads to its several promising and emerging engineering and industrial applications such as crystal growth process, compute storage devices, viscometry, jet motors, oceanography, and rotatory machinery. But this theory has taken a long time to accomplish significance. In 1921, von Karman [1] was the first to provide an efficient way of transforming and simplifying the PDEs into ODEs with constant angular velocity and approximated solution been obtained. Based on von Karman's concept Cochran and Goldstein [2] reconsidered the problem and calculated series solutions asymptotically, and the results are more accurate. The heat and mass transfer inside the boundary layer of non-Newtonian fluids is one of the major research topics in fluid mechanics because of its enormous industrial and manufacturing applications, such as the petroleum industry, polymer devolatilization fermentation, etc. Various non-Newtonian fluids obey numerous characteristics, such as paints, blood, emulsions, and cosmetic products. Sakiadis [3] studied the Blasius motion within the boundary layer due to constantly supplying speed surface. Erickson et al. [4] further extended it towards the polymer sector's implications to investigate the nature of the temperature. Crane [5] analytically studied the steady two-dimensional incompressible boundary layer flow on a stretching sheet. Rajagopal et al. [6] studied the second-order non-Newtonian fluid and calculated the boundary layer profiles through a similarity solution method. Chen [7] stated the upshots of the magnetic field parameter and suction/injection upon the convective heat transfer for non-Newtonian fluids using a surface heat flux model. Turkyilmazoglu [8] pondered the MHD fluid flow and heat transfer on a stretching and rotating disk. Srinivas et al. [9] evaluated the influences of thermal diffusion by applying the HAM method upon unsteady viscous MHD fluid flow between expanding or contracting rotatory porous disks with the help of viscous dissipation.

Stagnation point flow is a prominent part of the research in recent times. Stagnation axisymmetric point flow due to the rotation of disk has firstly presented by Hannah [10]. Wang [11] proposed the stagnation point flow for an off-centered rotating disk by numerically solving the proposed problem. It concluded that the shear due to non-alignment becomes complicated, but torque remains the same. Mustafa et al. [12] solved the three-dimensional MHD ferrofluid stagnation point flow on a stretchable rotating disk by considering magnetite, cobalt ferrite, and Mn-Zn ferrite as three ferrofluid particles. They concluded that by increasing the volume fraction parameter for magnetite, the radial velocity decreases while azimuthal and temperature increases. The authors investigated the stagnation point flow and heat transfer over the disk in [13-15]. Hayat et al. [16] studied the Carreau fluid along with thermal radiation and chemical reaction by examining the influences of stagnation point mixed convection flow and heat transfer with the occurrence of heat generation/absorption. They have concluded that the velocity and thermal thickness of the boundary layer decreases alongside the mixed convection parameter. Hayat et al. [17] further deal with the MHD Jeffrey fluid between two disks, which are rotatable and stretchable by applying the magnetic field with momentum equation and associated the heat source/sink and nonlinear radiation with energy equation. Hayat et al. [18] carried out the study for Casson Marangoni mixed convective fluid flow with the occurrence of nonlinear thermal radiation, Joule heating, viscous dissipation, and inclined magnetic field.

The fluid which fulfills the properties of shear-thinning and shear-thickening is known as power-law fluid. Von Karman's transformation has been enhanced towards the power-law fluids by Mitschka [19] in 1964. Mitschka and Ulbricht [20] calculated results for shear dependent viscosity by considering the flow due to disk rotation within the power-law index range from 0.2 to 1.5. Andersson et al. [21] extended the power-law index up to 2 by re-examining the work in [20] and settled with the outcome that the thickness of the boundary layer inflates by reducing the power-law index from 2 to 0.2. Andersson and Korte [22] successfully implemented the magnetic field on power-law fluids and observed that the magnetic field has more influence on shear-thinning than shear-thickening. In 2011, Ming et al. [23] enhanced the power-law index up to 2.5 and calculated the effects of a power-law fluid in

the temperature equation to assume that viscosity and thermal conductivity follow the property power-law. The authors like Ming et al. [24], Usman et al. [25], and Khan et al. [26] made valuable contributions in exploring power-law fluid in various aspects.

In recent times, nanofluid has been one of the most researched topics for scientists. That is why it caught the attention of researchers globally. The fluids like water, glycol, ethylene, and engine oil are poor heat transferring fluids as they have low thermal conductivity. To improve their heat transfer characteristics, nanofluid perform a vital role as they comprise metal. The term "nanofluid" was firstly introduced by Choi [27]. Several researchers have addressed the nanofluids such as Tiwari and Das [28], Ahmed et al. [29], Hafeez et al. [30], Acharya et al. [31], and Hayat et al. [32]. But, the aggregation of nanoparticles continuously remains a problem. Kuznetsov [33-36] presented an innovative concept by proposing a novel type of fluid consisting of nanoparticles and microorganisms. After obtaining the results, he found out that the mass transfer rate can be improved, and nanofluids stability enhanced upon adding microorganisms alongside the suspension. Chen et al. [37] studied the three-dimensional nanofluid within the boundary layer upon taking power-law stretching on it and consists of gyrotactic microorganisms. Ferdows et al. [38] debated the two-dimensional MHD power-law nanofluid containing gyrotactic microorganisms passing through a sheet that is stretching and vertically adjacent. Bhatti et al. [39] examined the swimming features of gyrotactic microorganisms in nanofluid upon considering the effects of MHD and porosity, passing through the stretchable surface. Aziz and Aly [40] have considered the exponentially stretching sheet through zero nanoparticles and convective heating and investigated the MHD power-law nanofluid within the boundary layer comprising gyrotactic microorganisms. Pal and Mondal [41] studied the bio-convection by considering the Powell Eyring nanofluid, which consists of gyrotactic microorganisms over a stretching sheet. Zaman and Gul [42] addressed the gyrotactic microorganisms in the MHD bio-convection flow of Williamson nanofluid concerning thermal radiation and Newtonian conditions. The exploration of gyrotactic microorganisms in diverse modes has been reported in [43-47].

The steady three-dimensional flow close to stagnation point inside the boundary layer and heat transfer of power-law nanofluid with the occurrence of MHD and nonlinear thermal radiation on a stretchable rotating disk filled with gyrotactic microorganisms is not investigated yet. Thus, it motivated us to investigate such a unique phenomenon by analyzing the influences of several pertinent parameters upon the velocity, temperature, concentration of nanoparticles, and motile density of microorganisms. With the aid of appropriate transformations, physically modeled PDEs are reduced to combined nonlinear ODEs and later tackled numerically through the shooting method. Entirely parametrical influence on the characteristics of Newtonian and non-Newtonian fluids has accentuated and been conducted.

2. Analysis of Physical Model

A three-dimensional stagnation point power-law nanofluid flow inside the boundary layer is assumed on a stretchable rotating disk filled with gyrotactic microorganisms. The heat transfer phenomenon in the presence of nonlinear thermal radiation is discussed. The proposed flow is said to be steady and axisymmetric. The velocity components (u, v, w) alongside the cylindrical coordinate system (r, θ^*, z) are chosen. The disk rotation along z-axis with respect to constant as well as angular velocity is taken. The disk is assumed to be stretching in the radial direction with a constant rate c and by the velocity $u = cr$. The variation in θ^* direction is ignored because of axisymmetric flow. The externally functional uniform magnetic field is maintaining the strength of B_0 and is employed perpendicularly in the z direction to the circulating disk. The gradient of pressure in z direction that is $\partial p/\partial z = 0$ [21].

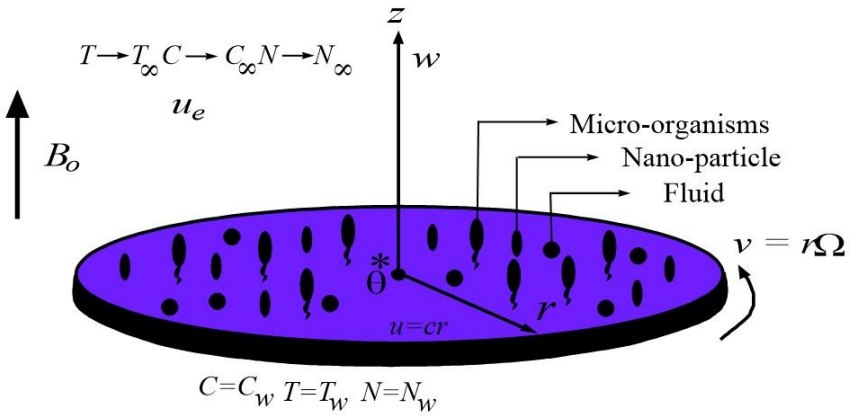

Fig. 1 The flow geometry of the proposed fluid flow phenomenon

Furthermore, Karman's transformation suggested that $\partial p/\partial r = 0$, it leads to the treatment of pressure as a constant within the entire boundary layer. The velocity which is outside of the boundary layer is specified as potential flow, and here it can be defined as $u_e = ar$. The constant temperature T_w, the concentration of nano-particles C_w and the motile density of microorganisms N_w are kept on the surface of the rotatory stretchable disk and which are out of boundary layer are placed at an ambient uniform temperature T_∞, the concentration of nano-particles C_∞ and motile density of microorganisms N_∞ with $T_w > T_\infty, C_w > C_\infty$ and $N_w > N_\infty$, at $z > 0$. The proposed equations of continuity, momentum, energy, the concentration of nanoparticles, and the motile density of microorganisms inside the boundary layer in terms of cylindrical coordinates can respectively be expressed as [23], [25], [37], and [50]:

$$\frac{\partial u}{\partial r} + \frac{u}{r} + \frac{\partial w}{\partial z} = 0 \tag{1}$$

$$u\frac{\partial u}{\partial r} - \frac{v^2}{r} + w\frac{\partial u}{\partial z} = u_e\frac{du_e}{dr} + \frac{1}{\rho_f}\frac{\partial}{\partial z}\left(\mu\frac{\partial u}{\partial z}\right) - \frac{\sigma_e B_0^2}{\rho_f}\left(u - u_e\right) \tag{2}$$

$$u\frac{\partial v}{\partial r} + \frac{uv}{r} + w\frac{\partial v}{\partial z} = \frac{1}{\rho_f}\frac{\partial}{\partial z}\left(\mu\frac{\partial v}{\partial z}\right) - \frac{\sigma_e B_0^2}{\rho_f}v \tag{3}$$

$$u\frac{\partial T}{\partial r} + w\frac{\partial T}{\partial z} = \frac{1}{\left(\rho c_p\right)_f}\left\{\frac{\partial}{\partial z}\left(\kappa\frac{\partial T}{\partial z}\right) - \frac{\partial q_r}{\partial z}\right\} + \tau D_B\left(\frac{\partial C}{\partial z}\frac{\partial T}{\partial z}\right) + \tau\frac{D_T}{T_\infty}\left(\frac{\partial T}{\partial z}\right)^2 \tag{4}$$

$$u\frac{\partial C}{\partial r} + w\frac{\partial C}{\partial z} = D_B\left(\frac{\partial^2 C}{\partial z^2}\right) + \frac{D_T}{T_\infty}\left(\frac{\partial^2 T}{\partial z^2}\right) \tag{5}$$

$$u\frac{\partial N}{\partial r} + w\frac{\partial N}{\partial z} = \frac{-bW_c}{\Delta C}\left\{N\frac{\partial^2 C}{\partial z^2} + \frac{\partial C}{\partial z}\frac{\partial N}{\partial z}\right\} + D_N\frac{\partial^2 N}{\partial z^2} \tag{6}$$

Where (u, v, w) represents velocity components in (r, θ^*, z) directions, u_e be the free stream velocity, ρ_f denotes the fluid density σ_e denotes effective electrical conductivity, B_0 represents the power of the uniform magnetic field, the power-law dynamic viscosity $\mu = \mu_f\left\{\left(\frac{\partial u}{\partial z}\right)^2 + \left(\frac{\partial v}{\partial z}\right)^2\right\}^{n-1/2}$ and thermal conductivity $k = k_f\left\{\left(\frac{\partial u}{\partial z}\right)^2 + \left(\frac{\partial v}{\partial z}\right)^2\right\}^{n-1/2}$ follows the power-law fluid characteristics [25] where μ_f and k_f be the nano-particles dynamic viscosity and thermal conductivity, $\left(\rho c_p\right)_f$ states the fluid specific heat at constant pressure,

T, C, and N indicates the temperature, concentration of nanoparticles, and motile density of microorganisms. The radiative heat flux in terms of Rosseland approximation is written as $q_r = -\frac{4\sigma^*}{3k^*}\frac{\partial T^4}{\partial z} = -\frac{16\sigma^* T^3}{3k^*}\frac{\partial T}{\partial z}$, here σ^* and k^* are the Stefan-Boltzmann constant and coefficient of mean absorption, $\tau = \frac{(\rho c)_p}{(\rho c)_f}$ expresses the effective ratio of heat capacity, D_B, D_T and D_N implies the Brownian diffusion, thermophoresis diffusion and microorganisms diffusivity coefficients, $-b$ be constant of Chemotaxis, $\Delta C = C_w - C_\infty$, W_c denotes the highest speed of the swimming cell.

The appropriate boundary conditions can be chosen as:

$$u = cr,\ \ v = \Omega r,\ \ w = 0,\ \ T = T_w,\ D_B\frac{\partial C}{\partial Z} + \frac{D_T}{T_\infty}\frac{\partial T}{\partial Z} = 0,\ N = N_w \text{ at } z = 0, \tag{7}$$

$$u = u_e \to ar,\ \ v = v_e \to 0,\ \ w = 0,\ \ T = T_\infty,\ C = C_\infty,\ N = N_\infty \text{ at } z = \infty, \tag{8}$$

3. Similarity Transformation

Upon introducing the similarity transformation for the proposed fluid flow problem as follows [25]:

$$\begin{aligned}
&\eta = z\left(\frac{c^{2-n}}{\nu_f}\right)^{1/(n+1)} r^{(1-n)/(1+n)},\ u = crF(\eta),\ v = crG(\eta),\\
&w = \left(\frac{c^{1-2n}}{\nu_f}\right)^{-1/(n+1)} r^{(n-1)/(n+1)}H(\eta),\ T = T_\infty + (T_w - T_\infty)\theta(\eta),\\
&C = C_\infty + (C_w - C_\infty)\varphi(\eta),\ N = N_\infty + (N_w - N_\infty)S(\eta).
\end{aligned} \tag{9}$$

By introducing (9) into (1-6), it leads to the following system of nonlinear ODEs as

$$H' = -2F - \frac{1-n}{1+n}\eta F' \tag{10}$$

$$F^2 - G^2 + \left(H + \frac{1-n}{1+n}\eta F\right)F' = \lambda^2 + \left\{F'\left[(F')^2 + (G')^2\right]^{(n-1)/2}\right\}' - M(F - \lambda) \tag{11}$$

$$2FG + \left(H + \frac{1-n}{1+n}\eta F\right)G' = \left\{G'\left[(F')^2 + (G')^2\right]^{(n-1)/2}\right\}' - MG \tag{12}$$

$$\left(H + \frac{1-n}{1+n}\eta F\right)\theta' = \frac{1}{Pr}\left\{\left[1 + Rd\left(1 + (\theta_w - 1)\theta\right)^3\right]\theta'\left[(F')^2 + (G')^2\right]^{(n-1)/2}\right\}' + \frac{N_b}{Pr_m}\theta'\varphi' + \frac{N_t}{Pr_m}\theta'^2 \tag{13}$$

$$\left(H + \frac{1-n}{1+n}\eta F\right)\varphi' = \frac{1}{Pr_m Le}\left(\varphi'' + \frac{N_t}{N_b}\theta''\right) \tag{14}$$

$$\left(H + \frac{1-n}{1+n}\eta F\right)S' = \frac{1}{LbPr_m}\left[S'' - Pe\left\{(\sigma + S)\varphi'' + \varphi' S'\right\}\right] \tag{15}$$

Where $'$ means the derivative, which is associated with dimensionless variable η and F, G, H represents the dimensionless radial, azimuthal and axial velocities, θ, φ, S describes the dimensionless temperature, the concentration of nanoparticles and the motile density of microorganisms, n is the power-law index.

The parameters which are helpful for the fluid to govern can be classified as:

$$\lambda = \frac{a}{c},\ M = \frac{B_0^2 \sigma_e}{c\rho_f},\ \alpha_f = \frac{k_f}{\left(\rho c_p\right)_f},\ Pr = \frac{\nu_f}{\alpha},\ Rd = \frac{16\sigma^* T_\infty^3}{3k_f k^*},\ \theta_w = \frac{T_w}{T_\infty},\ N_b = \frac{\tau D_B \left(C_w - C_\infty\right)}{\alpha_f},$$
$$N_t = \frac{\tau D_T \left(T_w - T_\infty\right)}{\alpha_f T_\infty},\ Pr_m = \frac{\nu^{\frac{2}{n+1}} \left(c^3 r^2\right)^{\frac{n-1}{n+1}}}{\alpha_f},\ Le = \frac{\alpha_f}{D_B},\ Lb = \frac{\alpha_f}{D_N},\ Pe = \frac{bW_c}{D_N},\ \sigma = \frac{N_\infty}{N_w - N_\infty}. \tag{16}$$

In which, λ is the velocity ratio parameter, M implies the parameter of the magnetic field, α_f means the thermal diffusivity, Pr indicates the Prandtl number, Rd specifies the radiation parameter, θ_w shows the temperature ratio parameter, N_b and N_t are the Brownian motion and thermophoresis parameters, Pr_m displays the modified Prandtl number, $Le, Lb, Pe,$ and σ demonstrates the Lewis number, bio-convection Lewis number, Peclet number, and the bio-convection parameter, respectively.

The corresponding transformed boundary conditions are:

$$F\left(0\right) = 1,\ G\left(0\right) = \omega,\ H\left(0\right) = 0,\ \theta\left(0\right) = 1,\ N_b \varphi'\left(0\right) + N_t \theta'\left(0\right) = 0,\ S\left(0\right) = 1, \tag{17}$$
$$F\left(\infty\right) = \lambda,\ G\left(\infty\right) = 0,\ \theta\left(\infty\right) = 0,\ \varphi\left(\infty\right) = 0,\ S\left(\infty\right) = 0. \tag{18}$$

The term $\omega = \frac{\Omega}{c}$ represents the rotation parameter.

4. Quantities of Interest

4.1 Skin friction coefficients

The surface drag forces or skin friction coefficients in radial C_{Fr} and azimuthal $C_{G\theta^*}$ directions are delineated as [25]

$$C_{Fr} = \frac{\tau_{rz}}{\rho_f \left(cr\right)^2},\ C_{G\theta^*} = \frac{\tau_{\theta^* z}}{\rho_f \left(cr\right)^2}, \tag{19}$$

The terms $\tau_{rz}, \tau_{\theta^* z}$ represents the shear stresses in radial and azimuthal directions, respectively. These stresses described as:

$$\tau_{rz} = \left[\mu\left\{\left(\frac{\partial u}{\partial z}\right) + \frac{1}{r}\left(\frac{\partial w}{\partial \theta^*}\right)\right\}\right]_{z=0} = \left[\mu\left(\frac{\partial u}{\partial z}\right)\right]_{z=0},\ \tau_{\theta^* z} = \left[\mu\left\{\left(\frac{\partial v}{\partial z}\right) + \frac{1}{r}\left(\frac{\partial w}{\partial \theta^*}\right)\right\}\right] = \left[\mu\left(\frac{\partial v}{\partial z}\right)\right]_{z=0}, \tag{20}$$

The non-dimensional form is

$$\mathrm{Re}_r^{\frac{1}{n+1}} C_{Fr} = \left[F'^2\left(0\right) + G'^2\left(0\right)\right]^{\frac{n-1}{2}} F'\left(0\right),\ \mathrm{Re}_r^{\frac{1}{n+1}} C_{G\theta^*} = \left[F'^2\left(0\right) + G'^2\left(0\right)\right]^{\frac{n-1}{2}} G'\left(0\right), \tag{21}$$

4.2 The heat transfer rates

The heat transfer rates or local Nusselt number Nu_r is given by [25]

$$Nu_r = \frac{rq_w}{k\left(T_W - T_\infty\right)}, \tag{22}$$

Where q_w is the surface heat flux and is defined as

$$q_w = \left[-k\frac{\partial T}{\partial z} + \left(q_r\right)_w\right]_{z=0} = -\left[\left\{1 + Rd\left(1 + \left(\theta_w - 1\right)\theta\right)^3\right\}k\frac{\partial T}{\partial z}\right]_{z=0}, \tag{23}$$

After introducing (9) into (23), we accomplish

$$\mathrm{Re}_r^{-\frac{1}{n+1}} Nu_r = -\left[1 + Rd\left(1 + \left(\theta_w - 1\right)\theta\left(0\right)\right)^3\right]\theta'\left(0\right), \tag{24}$$

4.3 The surface mass flux

The surface mass flux q_m is expressed as

$$q_m = -D_B\frac{\partial C}{\partial z}, \tag{25}$$

The dimensionless form is

$$\mathrm{Re}_r^{-\frac{1}{n+1}} q_m = -\varphi'\left(0\right), \tag{26}$$

4.4 The motile density number of microorganisms

Mathematically, the local motile density number of microorganisms can be written as

$$Nn_r = \frac{rq_n}{D_N\left(N_W - N_\infty\right)}. \tag{27}$$

Here, q_n denotes the surface flux of motile microorganisms, and it is stated as

$$q_n = \left[-D_N\frac{\partial N}{\partial z}\right]_{z=0}, \tag{28}$$

After introducing (9), we may write

$$\mathrm{Re}_r^{-\frac{1}{n+1}} Nn_r = -S'\left(0\right). \tag{29}$$

Here, $Re_r = \frac{r^2c^{2-n}}{\nu_f}$ refers to the local Reynolds number.

5. Shooting Method

The shooting method has been implemented to acquire the solution of highly nonlinear coupled ODEs. In the shooting method, the boundary value problem (BVP) must be converted into a first-order initial value problem (IVP). So, the BVP can be converted into the first-order IVP by defining the derivatives as:

$$y_1 = F,\ y_2 = F',\ y_3 = G,\ y_4 = G',\ y_5 = H,\ y_6 = \theta,\ y_7 = \theta',\ y_8 = \varphi,\ y_9 = \varphi',\ y_{10} = S,\ y_{11} = S'. \quad (30)$$

Thus, it will lead to the reduction of ODEs (10-15) into the 11 coupled first-order equations as IVP in the form of 11 functions y_N $(N = 1, 2, 3, \ldots, 11)$.

$$\begin{aligned}
&y_1' = y_2,\\
&y_2' = \frac{1}{n}.\left(y_2^2 + y_4^2\right)^{\frac{1-n}{2}}.\begin{Bmatrix}\left[1+(n-1)\left(y_2^2+y_4^2\right)^{-1}y_4^2\right]\left[y_1^2 - y_3^2 + \left(y_5 + \frac{1-n}{1+n}\eta y_1\right)y_2 - \lambda^2 + M\left(y_1 - \lambda\right)\right]\\ -(n-1)\left(y_2^2+y_4^2\right)^{-1}y_2y_4\left[2y_1y_3 + \left(y_5 + \frac{1-n}{1+n}\eta y_1\right)y_4 + My_3\right]\end{Bmatrix},\\
&y_3' = y_4,\\
&y_4' = \frac{1}{n}.\left(y_2^2 + y_4^2\right)^{\frac{1-n}{2}}.\begin{Bmatrix}\left[1+(n-1)\left(y_2^2+y_4^2\right)^{-1}y_2^2\right]\left[2y_1y_3 + \left(y_5 + \frac{1-n}{1+n}\eta y_1\right)y_4 + My_3\right]\\ -(n-1)\left(y_2^2+y_4^2\right)^{-1}y_2y_4\left[y_1^2 - y_3^2 + \left(y_5 + \frac{1-n}{1+n}\eta y_1\right)y_2 - \lambda^2 + M\left(y_1 - \lambda\right)\right]\end{Bmatrix},\\
&y_5' = -2y_1 - \frac{1-n}{1+n}\eta y_2,\\
&y_6' = y_7,\\
&y_7' = \frac{y_7}{\left[1+Rd\left(1+\left(\theta_w-1\right)y_6\right)^3\right]}\begin{Bmatrix}\left(y_2^2+y_4^2\right)^{\frac{1-n}{2}}\left[\left(Pr - \left(1+Rd\left(1+\left(\theta_w-1\right)y_6\right)^3\right)\frac{n-1}{n}\right)\left(y_5 + \frac{1-n}{1+n}\eta y_1\right) - \frac{Pr}{Pr_m}\left(N_by_8 + N_ty_7\right)\right]\\ -\left(\left(1+Rd\left(1+\left(\theta_w-1\right)y_6\right)^3\right)\frac{n-1}{n}\left(y_2^2+y_4^2\right)^{\frac{1-n}{2}-1}\right)\times\\ \left(y_1^2y_2 - y_2y_3^2 + 2y_1y_3y_4 - \lambda^2y_2 + M\left(y_2\left(y_1-\lambda\right) + y_3y_4\right)\right)\\ -3Rd\left(1+\left(\theta_w-1\right)y_6\right)^2\left(\theta_w-1\right)y_7\end{Bmatrix},\\
&y_8' = y_9,\\
&y_9' = Pr_mLe\left(y_5 + \frac{1-n}{1+n}\eta y_1\right)y_9 - \frac{N_t}{N_b}y_7',\\
&y_{10}' = y_{11},\\
&y_{11}' = LbPr_m\left(y_5 + \frac{1-n}{1+n}\eta y_1\right)y_{11} + Pe\left\{y_9y_{11} + \left(\sigma + y_{10}\right)y_9'\right\}.
\end{aligned} \quad (31)$$

The boundary conditions will take a new form:

$$\begin{aligned}
&y_1(0) = 1,\ y_2(0) = a_1,\ y_3(0) = \omega,\ y_4(0) = a_2,\ y_5(0) = 0,\ N_by_9(0) + N_ty_7(0) = 0, y_7(0) = a_3,\\
&y_8(0) = a_4,\ y_{10}(0) = a_5,\ y_1(\infty) = \lambda,\ y_3(\infty) = 0,\ y_6(\infty) = 0,\ y_8(\infty) = 0,\ y_{10}(\infty) = 0.
\end{aligned} \quad (32)$$

Where, $y_2(0) = a_1, y_4(0) = a_2, y_7(0) = a_3, y_8(0) = a_4$ and $y_{10}(0) = a_5$ indicates the missing initial conditions, which can be calculated from $y_1(\infty) = \lambda, y_3(\infty) = 0, y_6(\infty) = 0, y_8(\infty) = 0$ and $y_{10}(\infty) = 0$. For instance, to compute the values of a_3 and a_4 if we set the parameters as $Pr = Le = 10, n = \theta_w = 1.0, N_b = N_t = 0.1, Pr_m = 5,\ M = Rd = Lb = Pe = \sigma = 0,$ then after performing eight iterations with the shooting method with the step size 0.01, the calculated values of missing initial conditions $\left(-\theta'(0), -\varphi'(0)\right)$ are $(-a_3 = 0.9524, -a_3 = 2.1292\ )$ which are in good agreement with those in Ref. [48-49]. Similarly, if we change any of the involved parameters, we need to perform similar steps as above. Therefore, the adopted numerical scheme is beneficial for finding the solution of such highly nonlinear ODEs.

6. Results and Discussion

The coupled nonlinear ODEs (10-15) correspond to boundary conditions (17-18) and are numerically tackled through the shooting method. The effects of several types of pertinent parameters upon the boundary layer profiles are examined.

Table 1: Comparison of $-\theta'(0)$, when $Pr = Le = 10, n = \theta_w = 1.0, Pr_m = 5,\ M = Rd = Lb = Pe = \sigma = 0$.

N_b	N_t	$-\boldsymbol{\theta}(\mathbf{0})$		
		Present	Ref. [48]	Ref. [49]
0.1	0.1	0.9524	0.952493	0.9524
	0.2	0.6933	0.693282	0.6932
	0.3	0.5202	0.520173	0.5201
	0.4	0.4027	0.402662	0.4026
	0.5	0.3211	0.321125	0.3211
0.3	0.1	0.2522	0.252242	0.2522
	0.2	0.1817	0.181664	0.1816
	0.3	0.1356	0.135567	0.1355
	0.4	0.1047	0.104652	0.1046
	0.5	0.0833	0.083334	0.0833
0.5	0.1	0.0543	0.054284	0.0543
	0.2	0.0390	0.039063	0.0390
	0.3	0.0291	0.029153	0.0291
	0.4	0.0225	0.022513	0.0225
	0.5	0.0179	0.017933	0.0179

Table 2: Comparison of $-\varphi'(0)$, when $Pr = Le = 10, n = \theta_w = 1.0, Pr_m = 5,\ M = Rd = Lb = Pe = \sigma = 0$.

N_b	N_t	$-\boldsymbol{\varphi}(\mathbf{0})$		
		Present	Ref. [48]	Ref. [49]
0.1	0.1	2.1292	2.129151	2.1294
	0.2	2.2736	2.273639	2.2740
	0.3	2.5282	2.528152	2.5286
	0.4	2.7946`	2.794607	2.7952
	0.5	3.0345	3.034519	3.0351
0.3	0.1	2.4099	2.409896	2.4100
	0.2	2.5149	2.514845	2.5150
	0.3	2.6086	2.608648	2.6088
	0.4	2.6874	2.687421	2.6876
	0.5	2.7517	2.751676	2.7519
0.5	0.1	2.3835	2.383477	2.3836
	0.2	2.4467	2.446704	2.4468
	0.3	2.4983	2.498260	2.4984
	0.4	2.5398	2.539748	2.5399
	0.5	2.5730	2.572979	2.5731

A tabular comparison and comprehensive graphical analysis of outcomes is made in the form of radial velocity F, azimuthal velocity G, temperature θ, nano-particles concentration φ and motile density of microorganisms S, skin friction in radial C_{Fr} as well as in azimuthal $C_{G\theta^*}$ directions, local Nusselt number Nu_r, mass flux $-\varphi(0)$ and local motile density number of microorganisms Nn_r with respect to emerging parameters such as magnetic field parameter M, power-law index n, Prandtl number Pr, radiation parameter Rd, temperature ration parameter θ_w, Brownian motion parameter N_b, the thermophoresis parameter N_t, modified Prandtl number Pr_m, Lewis number Le, Bioconvection Lewis number Lb, Peclet number Pe, the bio-convection parameter σ. A comparison is

established for Newtonian fluid $n = 1$, shear-thinning $n < 1$, shear-thickening $n > 1$. Tables 1-3 are drawn to validate the proposed numerical technique by selecting the appropriate values of the parameters from the literature. It can be seen that the results are converging significantly with the previously existing literature. The numerical values of skin friction coefficients in radial and azimuthal directions are calculated for different values of M, ω, and λ in table 4.

Table 3: Comparison of $F'(0), -G'(0), -H(\infty), -\theta'(0)$, when $Pr = 1, \theta_w = 1.0,\ N_b = 0.1, Pr_m = 5,\ M = Rd = N_t = Le = Lb = Pe = \sigma = 0$.

n	$F'(0)$		$-G'(0)$		$-H(\infty)$		$-\theta'(0)$	
	Present	Ref. [23]	Present	Ref. [23]	Present	Ref. [23]	Present	Ref. [23]
2.5	0.5623	0.56236	0.6096	0.60967	0.5420	0.54200	0.3998	0.39980
2.2	0.5531	0.55319	0.6056	0.60566	0.5655	0.56553	0.3965	0.39655
2.0	0.5467	0.54676	0.6032	0.60327	0.5876	0.58765	0.3939	0.39392
1.7	0.5366	0.53664	0.6009	0.60091	0.6366	0.63662	0.3897	0.38970
1.5	0.5291	0.52919	0.6009	0.60099	0.6782	0.67828	0.3885	0.38859
1.3	0.5215	0.52150	0.6034	0.60346	0.7359	0.73591	0.3891	0.38910
1.0	0.5102	0.51021	0.6159	0.61591	0.8823	0.88230	0.3963	0.39632
0.8	0.5038	0.50381	0.6360	0.63608	1.0592	1.05929	0.4110	0.41108
0.5	0.5005	0.50058	0.7132	0.71322	1.5439	1.54389	0.4792	0.47917

Table 4: The numerical values of skin friction coefficients for diverse M, ω, and λ when $Rd = 2.0, \theta_w = 1.3, Pr = 7.0, Pr_m = 5.0, N_t = 1.3, N_b = 0.6, Lb = 2.0, Le = Pe = 3.0$, and $\sigma = 1.0$.

M	ω	λ	$Re_r^{\frac{1}{n+1}} C_{Fr}$			$Re_r^{\frac{1}{n+1}} C_{G\theta^*}$		
			$n = 0.8$	$n = 1.0$	$n = 1.2$	$n = 0.8$	$n = 1.0$	$n = 1.2$
1	0.5	1.5	1.1370	1.1523	1.1638	-1.0704	-1.0809	-1.0891
0.0			1.0363	1.0414	1.0455	-0.9619	-0.9628	-0.9641
0.5			1.0880	1.0982	1.1058	-1.0178	-1.0234	-1.0280
2.0			1.2283	1.2541	1.2736	-1.1675	-1.1883	-1.2041
1.0	0.2		1.1426	1.1216	1.1039	-0.4411	-0.4321	-0.4246
	0.6		1.1393	1.1684	1.1914	-1.2707	-1.2975	-1.3193
	1.0		1.1771	1.2616	1.3329	-2.0382	-2.1670	-2.2770
	0.5	1.2	0.4701	0.4606	0.4525	-1.0689	-1.0418	-1.0199
		1.4	0.9133	0.9141	0.9138	-1.0711	-1.0680	-1.0650
		1.6	1.3622	1.3980	1.4265	-1.0695	-1.0937	-1.1134
		2.0	2.2811	2.4517	2.5976	-1.0685	-1.1437	-1.2085

6.1 Influence of the parameter of the magnetic field

Figures 2-3 are sketched to show the upshots of magnetic field parameter M on radial F and azimuthal G velocities for Newtonian fluid $n = 1$, shear-thinning $n < 1$ and for shear-thickening $n > 1$ by setting other parameters as $\omega = 0.5,\ \lambda = 1.5, Pr = 7, Rd = 2, \theta_w = 1.3, N_b = 0.6, N_t = 1.3, Pr_m = 5, Le = 3, Lb = 2, Pe = 3, \sigma = 1$. A cross-type of flow has been observed for F and G. The radial, as well as azimuthal velocities, decays as M surges. The occurrence of the magnetic field in an electrically conducting fluid introduces Lorentz force, which behaves against the flow if it is applied perpendicularly. Such type of resisting force reduces the fluid velocity within the boundary layer. Also, by the rise in M, there is no significant influence on other profiles except velocities because the magnetic forces are mainly connected with velocities.

6.2 Influence of the power-law index

The effects of the power-law index n upon the radial, azimuthal components of the velocity (F, G), temperature θ, the concentration of nano-particles φ, and the motile density of microorganisms S against the similarity variable η for Newtonian and non-Newtonian fluids are displayed in figures (4-8). The other involved parameters are scaled as $\omega = 0.5,\ \lambda = 1.5,\ M = 1, Pr = 7, Rd = 2, \theta_w = 1.3, N_b = 0.6, N_t = 1.3, Pr_m = 5, Le = 3, Lb = 2, Pe = 3,\ \sigma = 1$. A cross-sectional flow is produced for all profiles except S. It can be observed that with the rise in n it leads to the reduction in F, G, θ, and S. Because increasing n propelled to enhance the momentum layers as a result frictional forces boosted, which yields resistance near the disk. The thickness of the boundary layer reduces with the upsurge in the power-law index.

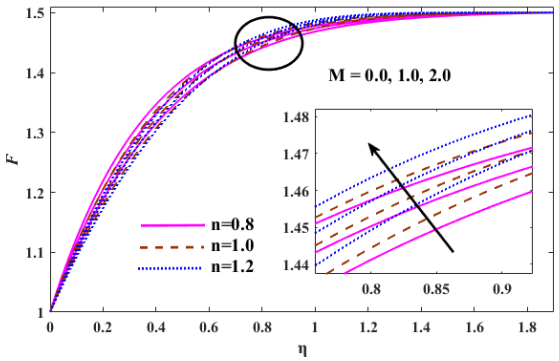

Fig 2. Influence of M upon F.

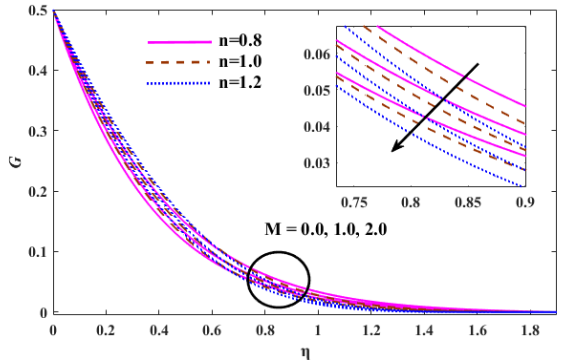

Fig 3. Influence of M upon G.

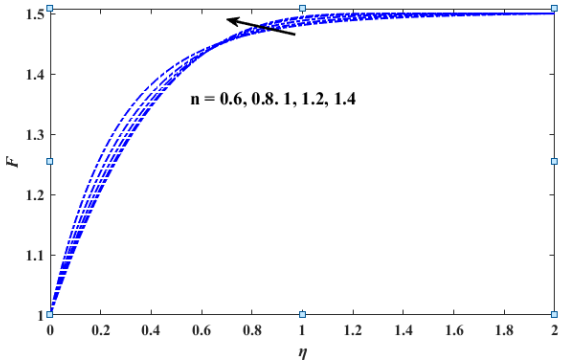

Fig 4. Influence of n upon F.

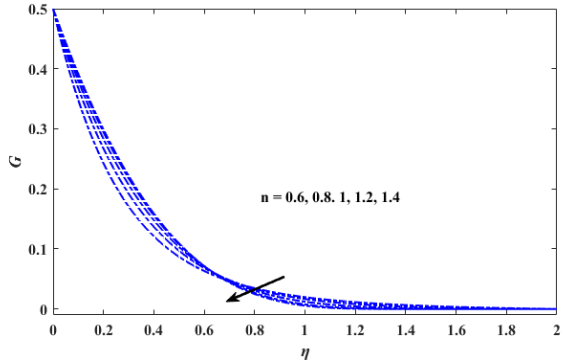

Fig 5. Impact of n upon G.

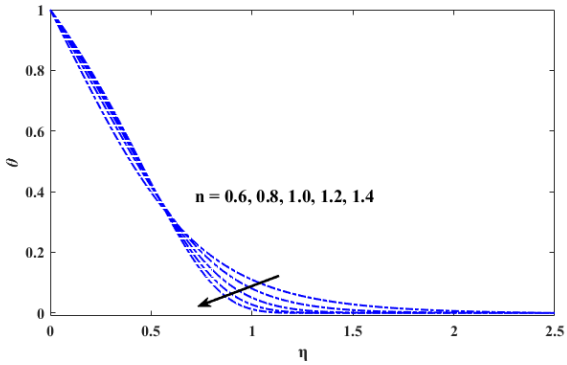

Fig 6. Impact of n upon θ.

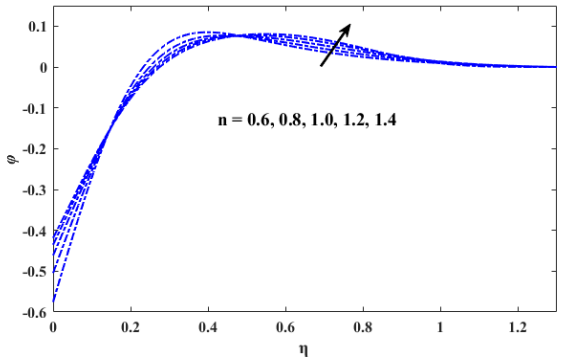

Fig 7. Impact of n upon φ.

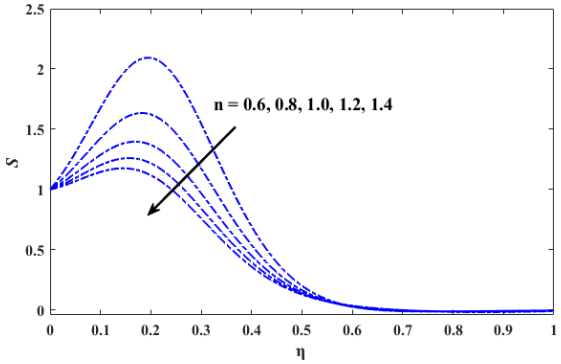

Fig 8: Effects of n upon S.

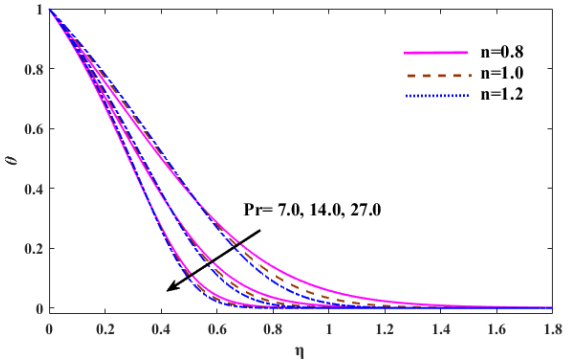

Fig 9: Influence of Pr upon θ.

6.3 Upshots of the Prandtl number

Figure 9 displayed the upshots of Prandtl number Pr upon the profile of temperature θ for Newtonian and non-Newtonian fluids when $\omega = 0.5,\ \lambda = 1.5, M = 1, Rd = 2, \theta_w = 1.3, N_b = 0.6, N_t = 1.3, Pr_m = 5, Le = 3, Lb = 2, Pe = 3,\ \sigma = 1$. It is noted that upon enhancing the Prandtl number, the temperature reduces. The fact behind this is that the Prandtl number associates the momentum and thermal diffusivities that is why enhancement in the Prandtl number leads to the diminution in the thermal diffusivity due to which temperature decreases. The boundary layer thickness reduces with the rise in the Prandtl number. The effects for shear-thinning fluid $n = 0.8$ are more noticeable in comparison with that of shear thickening $n = 1.2$.

6.4 Influence of linear and nonlinear radiations

The upshots of linear ($\theta_w = 1.0$) and nonlinear $\theta_w > 1.3$ radiations on temperature θ along η have been captured in figure 10 by fixing $\omega = 0.5,\ \lambda = 1.5, M = 1, Pr = 7, Rd = 2, N_b = 0.6, N_t = 1.3, Pr_m = 5, Le = 3, Lb = 2, Pe = 3,\ \sigma = 1$. It should be noted here that θ_w states the temperature comparison between the larger wall to that of the ambient one. The augmentation in θ_w consequently, temperature inflates. The nonlinear radiation increases the temperature for shear-thinning fluid $n = 0.8$ dramatically than linear radiation. Physically, the rise in θ_w leads to an extremely large fluid temperature than from ambient temperature because of which the thermal state of the temperature increases. Further, the distribution of temperature for the nonlinear stretching surface is significantly affected than by the linear stretching surface for rising θ_w. Hence, the boundary layer thickness increases as θ_w increases, but it decreases as n increases.

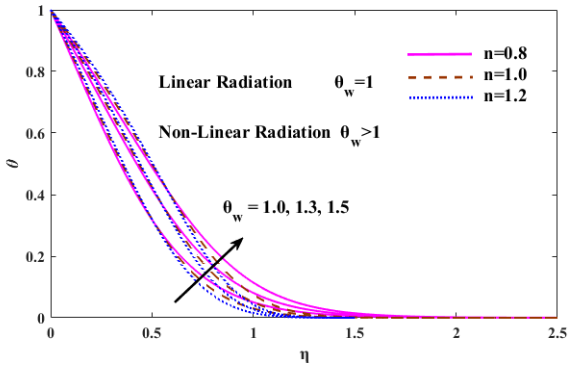

Fig 10: Influence of θ_w upon θ.

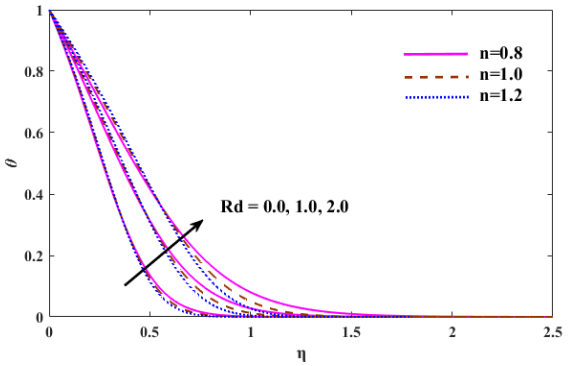

Fig 11: Influence of Rd upon θ.

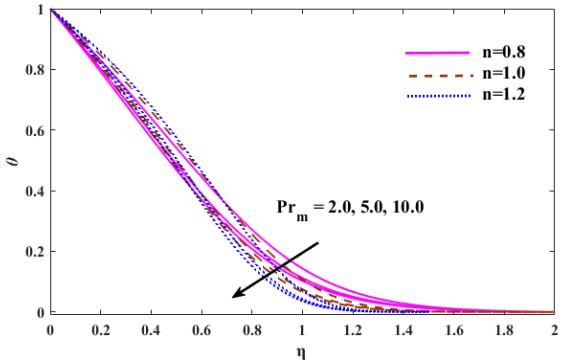

Fig 12: Influence of Pr_m upon the dimensionless temperature θ.

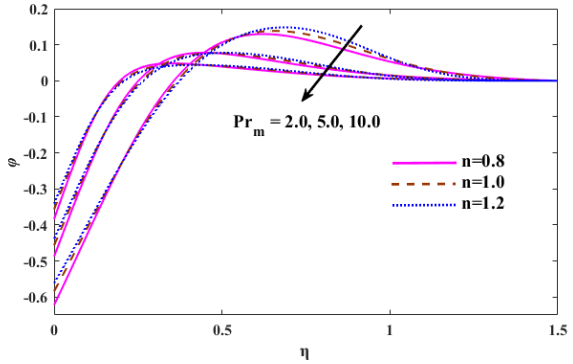

Fig 13: Effects of Pr_m on the dimensionless nanoparticle concentration φ.

6.5 Influence of thermal radiation

Figure 11 emphasis the effects of thermal radiation parameter Rd on temperature θ profile by scaling $\omega = 0.5,\ \lambda = 1.5, M = 1, Pr = 7, \theta_w = 1.3, N_b = 0.6, N_t = 1.3, Pr_m = 5, Le = 3, Lb = 2, Pe = 3,\ \sigma = 1$. After the examination of figure 11, the elevation in the behavior of temperature can be observed. It is physically stated as the augmentation in the thermal radiation parameter Rd results in a reduction within the coefficient of mean absorption, which delivers further heat in the direction of the fluid, causing the rise in temperature inside the boundary layer. Therefore, upon boosting Rd the boundary layer thickness for shear-thickening fluid $n = 1.2$ is smaller than Newtonian $n = 1$ and shear-thinning $n = 0.8$ fluids.

6.6 Influence of modified Prandtl number

Figures 12-14 accentuated the upshots of modified Prandtl number Pr_m upon the profiles of temperature θ, the concentration of nano-particles φ and motile density of microorganisms S for Newtonian $n = 1$, Shear-thinning $n = 0.8$, and Shear-thickening $n = 1.2$ fluids as $\omega = 0.5,\ \lambda = 1.5, M = 1, Pr = 7,\ Rd = 2, \theta_w = 1.3, N_b = 0.6, N_t = 1.3,\ Le = 3, Lb = 2, Pe = 3,\ \sigma = 1$. It can be witnessed that all profiles are decreasing along with the similarity variable for the diverse values of Pr_m. It is because the Prandtl number states momentum diffusivity to thermal diffusivity. It also signifies how rapidly the thermal diffusion has taken place than momentum diffusion. It further refers to the relative thickness of the thermal boundary layer to that of the momentum boundary layer. When the Prandtl number is smaller, it identifies the domination of thermal diffusion over momentum diffusion.

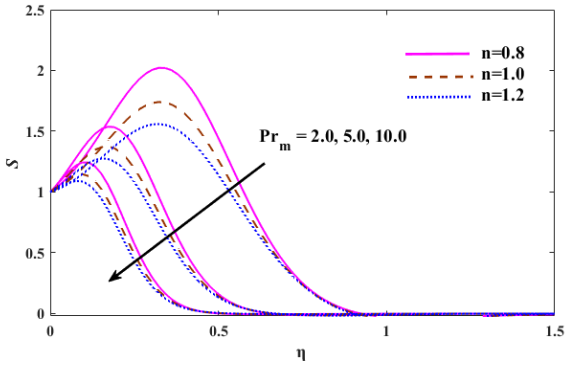

Fig 14: Influence of Pr_m upon S.

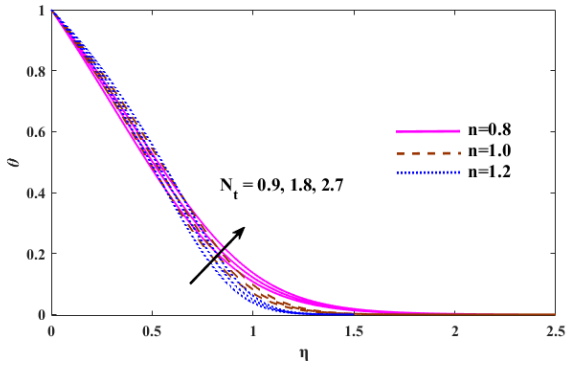

Fig 15: Impact of N_t on θ.

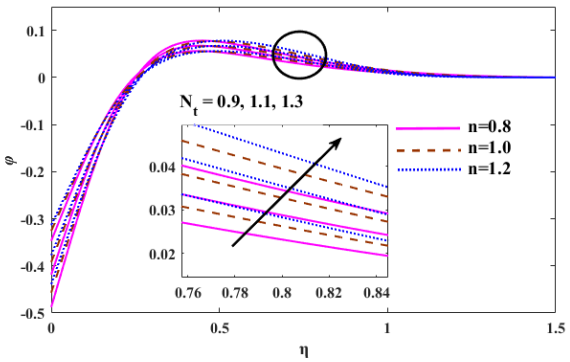

Fig 16: Impact of N_t on φ.

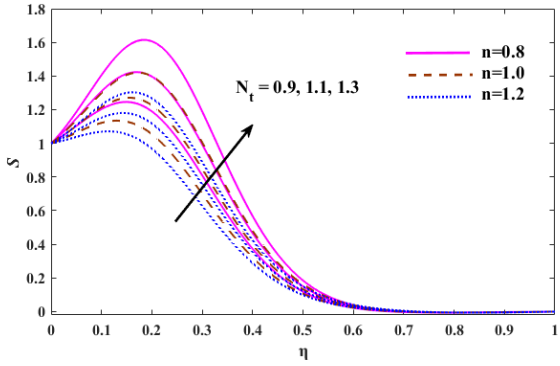

Fig 17: Effects of N_t upon S.

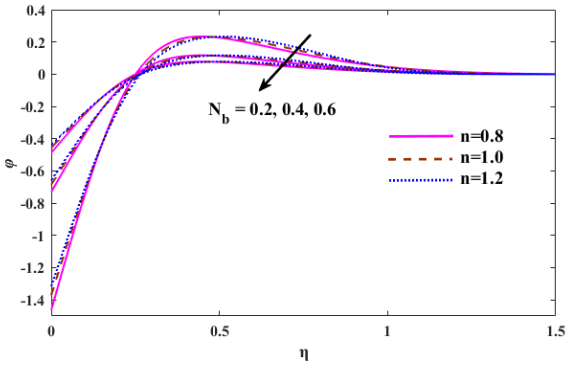

Fig 18: Effects of N_b on φ.

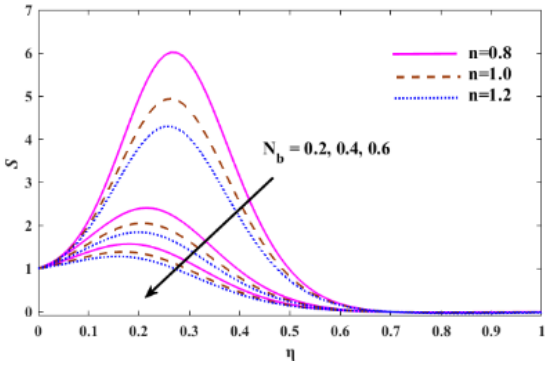

Fig 19: Effects of N_b upon S.

More preciously, for the proposed fluid flow problem, the conditions for the flow remain unchanged, if we intend to obtain a higher heat transfer rate, we have to consider the fluid with a lower Prandtl number. Moreover, the increase in the parameter Pr_m implies the reduction in the boundary layer.

6.7 Influence of Thermophoresis parameter

The upshots of the thermophoresis parameter N_t upon the profiles of temperature θ, nano-particles concentration φ and the motile density of microorganisms S are illustrated in figures (15-17) as $\omega = 0.5,\ \lambda = 1.5, M = 1, Pr = 7, Rd = 2, \theta_w = 1.3, N_b = 0.6, Pr_m = 5,\ Le = 3, Lb = 2, Pe = 3,\ \sigma = 1$. The profiles are increasing along the dimensionless similarity variable η for rising values of N_t. The N_t can either be positive or negative. Positivity of N_t means hot surface and negativity of N_t refers to the cold surface. In thermophoresis, the small fluid particles move back from the hot surface to the cold surface. Thus, the fluid particles dragged back in the thermophoresis process from the heated surface due to which temperature increases. Upon rising the N_t causes an increase in the number of nanoparticles because of which nano-particles concentration increases. The thickness of the boundary layer increases as N_t increases.

6.8 Influence of Brownian motion parameter

The concentration of nano-particles φ and motile density S are decaying in figures 18-19 for the diverse values of the Brownian motion parameter N_b. The profiles are plotted against the dimensionless similarity variable η while setting other quantities as $\omega = 0.5,\ \lambda = 1.5, M = 1, Pr = 7,\ Rd = 2,\ \theta_w = 1.3,\ N_t = 1.3,\ Pr_m = 5,\ Le = 3,\ Lb = 2,\ Pe = 3,\ \sigma = 1$. During Brownian motion, an unsystematic motion of the liquid particles occurs, and when Brownian motion rises, the unsystematic motion of liquid particles

is increased. Thus, when N_b upsurges, the particles collide and create the resistance in the nanoparticles due to which the concentration of nanoparticles and boundary layer thickness declines.

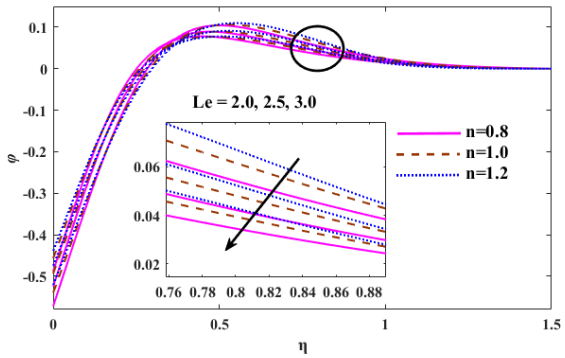

Fig 20: Impact of Le on φ.

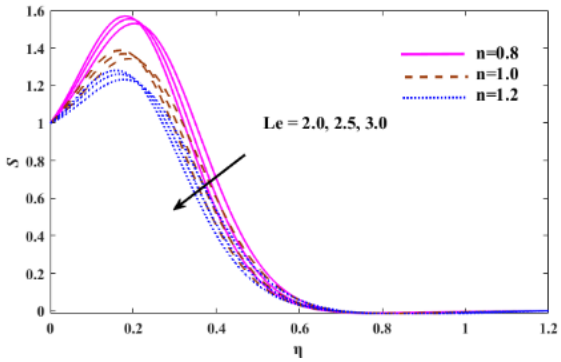

Fig 21: Effects of Le upon S.

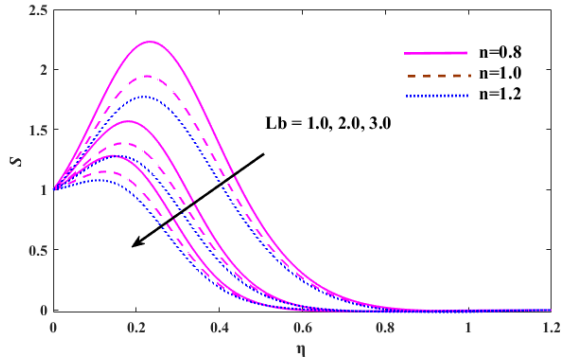

Fig 22: Effects of Lb upon S.

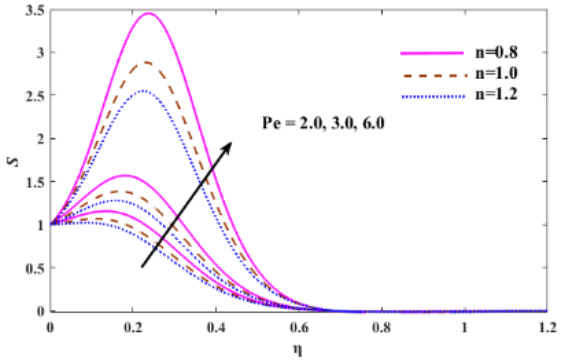

Fig 23: Effects of Pe upon S.

6.9 Influence of Lewis number

A decreasing trend can be noticed from figures 20-21 for nanoparticles concentration φ and motile density of microorganisms S for some values of Lewis number Le. The shear-thinning $n = 0.8$ and shear-thickening $n = 1.2$ fluids are decreasing along η for increasing Le. The dimensionless Lewis number Le can be expressed as the ratio of momentum and mass diffusivities. Whenever there are the processes of momentum and mass diffusion convection, the fluid flow can be characterized by the help of Lewis number. It is related to the relative thickness of the hydrodynamic layer and the boundary layer of mass transfer. Increasing Le indicates the existence of strong molecular motions which may enhance the temperature but owns a weaker D_B as Le is inversely proportional to the coefficient of Brownian diffusion D_B which let the particles to diffuse deeply within the fluid. Thus, diffusivity decreases, and it leads to a decline in nanoparticle concentration φ.

6.10 Influence of bio-convection Lewis number

Figure 22 deliberated the effects of bio-convection Lewis number Lb on the motile density of microorganisms S when $\omega = 0.5,\ \lambda = 1.5, M = 1, Pr = 7,\ Rd = 2, \theta_w = 1.3,\ N_b = 0.6, N_t = 1.3, Pr_m = 5, Le = 3, Pe = 3,\ \sigma = 1$. A decreasing trend can be observed for the profile of S along the η. The profile shows a rapid decrease in S. It is because of the reason that the parameter Lb opposes the motion of the fluid. The diffusivity of microorganisms declines by increases in the values of Lb and therefore, the motile density of microorganisms and thickness of the boundary layer decreases.

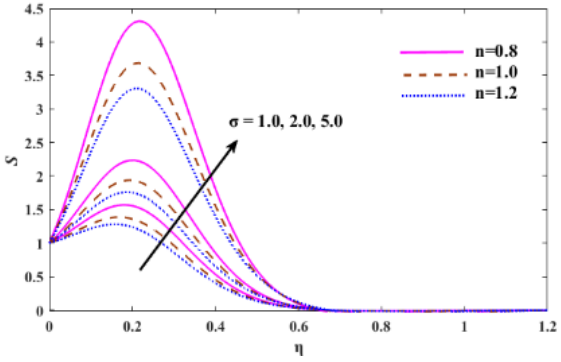

Fig 24: Effects of σ upon S.

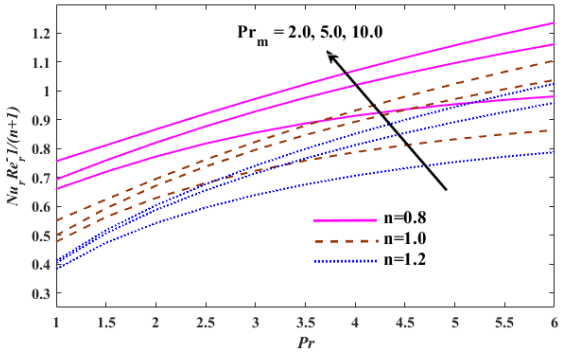

Fig 25. Local Nusselt number against Pr for different Pr_m

6.11 Influence of Peclet number

The influence of Peclet number Pe upon the motile density S are illustrated in figure 23 by assuming $\omega = 0.5,\ \lambda = 1.5, M = 1, Pr = 7,\ Rd = 2, \theta_w = 1.3,\ N_b = 0.6, N_t = 1.3, Pr_m = 5, Le = 3,\ Lb = 2, \sigma = 1$. The parameter Pe is the ratio of convected thermal energy to the fluid and convected thermal energy within the fluid. The motile density and the thickness of the boundary layer are increased with the rising Pe along η. It is because upon rising Pe the diffusivity of microorganisms reduces due to which S accelerates consequently. The effects on shear-thinning fluid $(n = 0.8)$ are more perceptible.

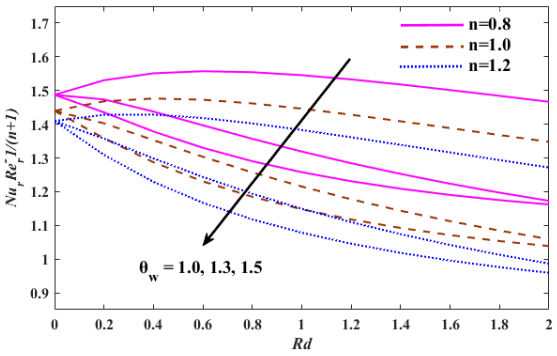

Fig 26. Local Nusselt number against Rd for different θ_w.

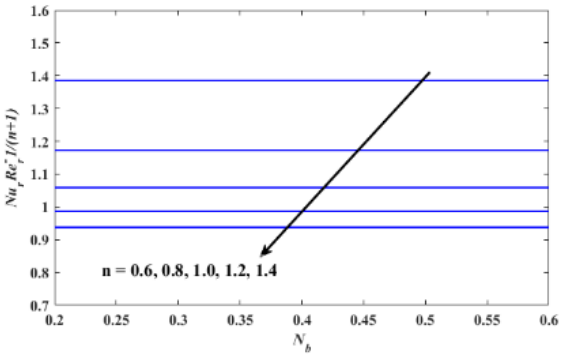

Fig 27. Local Nusselt number against N_b for $n = 0.6, 0.8, 1.0, 1.2, 1.4$

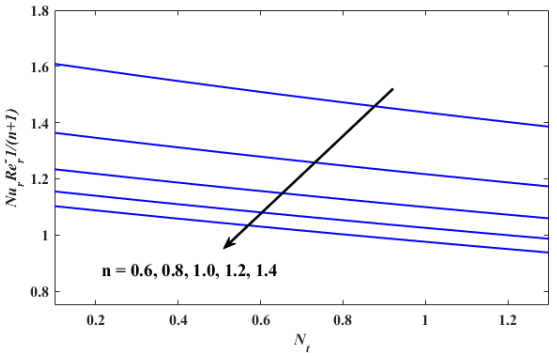

Fig 28. Local Nusselt number against N_t for $n = 0.6, 0.8, 1.0, 1.2, 1.4$

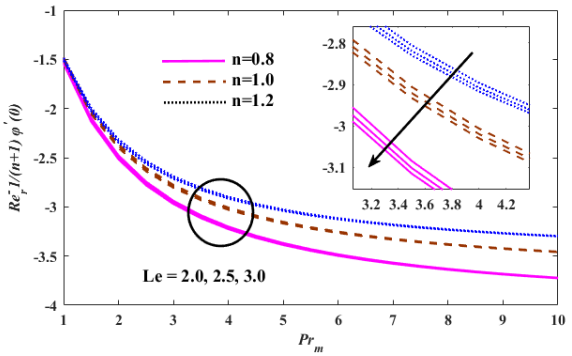

Fig 29. Non-dimensinal mass flux against Pr_m for $Le = 2.0, 2.5, 3.0$.

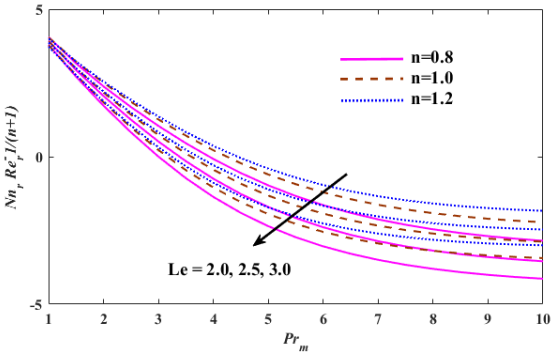

Fig 30. Local density number against Pr_m for $Le = 2.0, 2.5, 3.0$.

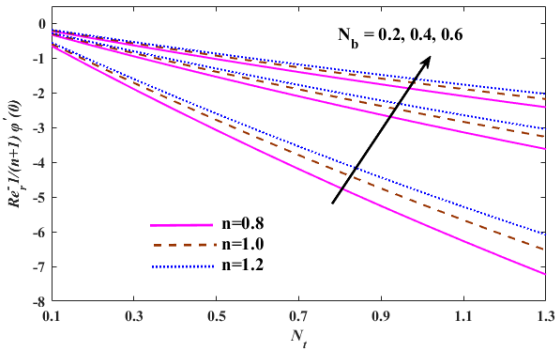

Fig 31. Non-dimensional mass flux against N_t for $N_b = 0.2, 0.4, 0.6$.

6.12 Influence of bio-convection parameter

Figure 24 displays the effects of the bio-convection parameter σ upon the motile density of microorganisms S for Newtonian and non-Newtonian fluids by giving suitable values to other parameters as $\omega = 0.5,\ \lambda = 1.5, M = 1, Pr = 7,\ Rd = 2, \theta_w = 1.3,\ N_b = 0.6, N_t = 1.3, Pr_m = 5, Le = 3,\ Lb = 2,\ Pe = 3$. The profile of S and thickness of the boundary layer increases with the increase in σ along η. The concentration of microorganisms enhances within the ambient fluid upon increasing σ and deduction in the density profile. The thickness of the boundary layer is thicker for shear-thinning $n = 0.8$.

6.13 Local Nusselt number against Prandtl number

The local Nusselt number Nu_r is plotted in figure 25 alongside the Prandtl number Pr for various modified Prandtl number Pr_m. The effects on Newtonian and non-Newtonian fluids can be observed by fixing other quantities as $\omega = 0.5, \lambda = 1.5,\ M = 1, Rd = 2, \theta_w = 1.3, N_b = 0.6, N_t = 1.3,\ Le = 3, Lb = 2, Pe = 3,\ \sigma = 1$. The Nu_r is increasing along Pr for different Pr_m. The local Nusselt number is in increasing trend. Since the Prandtl numbers are connected with momentum and thermal diffusivities, an increase in Pr causes a decrease in these diffusivities. Thus heat transfer rates are improved. It can be further observed that the rise in Pr_m the shear-thinning fluid $n = 0.8$ is larger from shear-thickening fluid $n = 1.2$.

6.14 Local Nusselt number against the radiation parameter

Figure 26 displays the behavior of local Nusselt number Nu_r with the aim of linear $\theta_w = 1$ and nonlinear $\theta_w > 1$ radiations for Newtonian and non-Newtonian fluids along with radiation parameter when $\omega = 0.5,\ \lambda = 1.5,\ M = 1,\ Pr = 7,\ Pr_m = 5, N_b = 0.6, N_t = 1.3,\ Le = 3, Lb = 2, Pe = 3,\ \sigma = 1$. The influence of radiation leads to a decline in the Nu_r. The rise in Rd means the diminution in the mean absorption coefficient because of which heat transfer rates decays. The reduction for nonlinear radiation is more considerable from linear radiation. The shear-thickening is smaller for linear and nonlinear radiations than that of shear-thinning.

6.15 Local Nusselt number against the Brownian motion and Thermophoresis parameters

The local Nusselt number Nu_r for some values of the power-law index n along with the parameters of Brownian motion N_b and thermophoresis N_t are drawn in figures 27-28 when $\omega = 0.5,\ \lambda = 1.5,\ M = 1,\ Pr = 7,\ Rd = 2,\ \theta_w = 1.3,\ Pr_m = 5,\ Le = 3,\ Lb = 2,\ Pe = 3,\ \sigma = 1$. A declining pattern can be observed in both cases, and this declination is on an extreme level for shear-thickening $n > 1$ fluid. The collision of the particles in the Brownian motion case causes resistance in nanoparticles. In the case of

thermophoresis, the fluid particles move from hot to the cold surface. Thus, these factors are responsible for decreasing heat transfer rates.

6.16 Mass flux and local density number against modified Prandtl number

The mass flux $-\varphi(0)$ and local motile density number Nn_r are decaying in figures 29-30 along with the modified Prandtl number Pr_m for rising values of Lewis number Le upon fixing $\omega = 0.5,\ \lambda = 1.5, M = 1, Pr = 7, Rd = 2, \theta_w = 1.3, N_b = 0.6, N_t = 1.3,$ $Lb = 2, Pe = 3,\ \sigma = 1$. The Lewis number Le is an inverse relationship with Brownian diffusion D_B, the higher Le cause D_B weaker because of which particles diffuses deeper in the fluid. Therefore based on this concept, the profiles of mass flux and local motile density number decays. In both situations, the shear-thinning $n = 0.8$ fluid diminishes more than Newtonian $n = 1$ and shear-thickening $n = 1.2$ fluids.

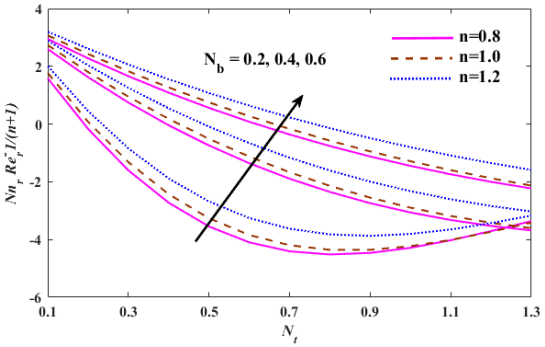

Fig 32. Local density number against N_t for $N_b = 0.2, 0.4, 0.6$.

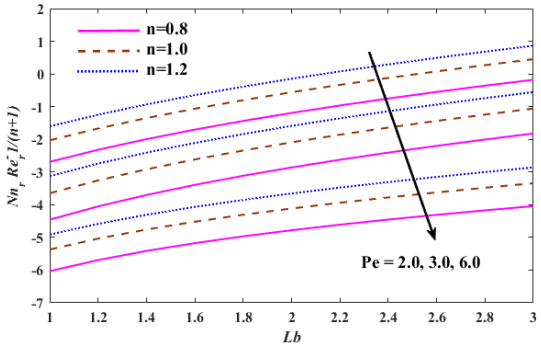

Fig 33. Local density number against Lb for $Pe = 2.0, 3.0, 6.0$.

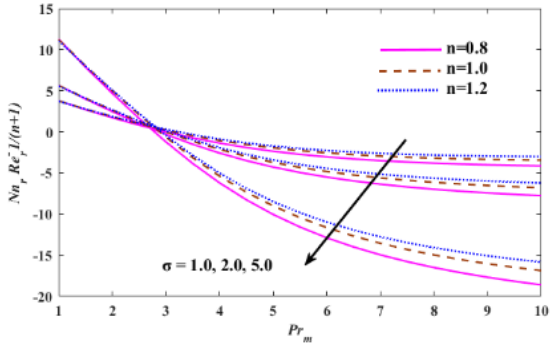

Fig 34. Local density number against Pr_m for $\sigma = 1.0, 2.0, 5.0$.

6.17 Mass flux and local density number against Thermophoresis parameter

Figures 31-32 are plotted to scrutinize the behaviors of mass flux $-\varphi(0)$ and local motile density number of microorganisms Nn_r against the thermophoresis parameter N_t for sundry values of Brownian motion parameter N_b when $\omega = 0.5,\ \lambda = 1.5, M = 1, Pr = 7, Rd = 2, \theta_w = 1.3, Pr_m = 5, Le = 3, Lb = 2, Pe = 3,\ \sigma = 1$. It can be witnessed that the mass flux and local motile density number are boosting for rising values of the Brownian motion parameter. The number of nanoparticles is increased upon rising the N_t because of which the mass flux and local motile density number increases. The shear-thickening is larger from Newtonian and shear-thinning.

6.18 Local density number against bio-convection Lewis number and modified Prandtl number

The local motile density number Nn_r is drawn along the bio-convection Lewis number Lb and modified Prandtl number Pr_m in figures 33-34 for diverse values of Peclet number Pe and bio-convection parameter σ respectively when $\omega = 0.5,\ \lambda = 1.5, M = 1, Pr = 7, Rd = 2, \theta_w = 1.3,\ N_b = 0.6, N_t = 1.3, Le = 3$. The rise in Pe and σ the local density number decreases in both figures, and this reduction is more evident for shear-thinning fluid. Physically, the parameter Lb opposes the fluid motion, and upon rising Pe the microorganisms diffusivity reduces, which are responsible for the reduction in the distribution of local motile density number.

7. Conclusion

In this research study, the heat transfer analysis phenomenon has been conducted for a steady three-dimensional stagnation point power-law nanofluid flow with the uniformly operated magnetic field and nonlinear thermal radiation on a rotatory stretchable disk which is filled with gyrotactic microorganisms. The physically modeled PDEs are reduced to a system of highly nonlinear coupled ODEs, which are numerically tackled through the shooting method. The upshots of several types of promising parameters upon the profiles of velocities, temperature, the concentration of nanoparticles, and gyrotactic microorganisms for Newtonian and non-Newtonian fluids are investigated in tabular and graphical forms. Furthermore, the effects of physically interesting quantities are also analyzed. Thus from a comprehensive exploration, the following conclusions can be depicted:

- The rise in M causes an increase in radial velocity, but it reduces azimuthal velocity.
- The radial velocity and concentration are enhanced while azimuthal velocity, temperature, and microorganisms diminished for the rising n.
- The temperature declines for augmented Pr and Pr_m but it increases for θ_w and Rd.
- The concentration and microorganisms are decreased for rocketing Pr_m and along η.
- An increasing trend is noted for temperature, concentration, and microorganisms for diverse N_t. The profiles of concentration and microorganisms decay for increasing N_b.
- Upon boosting Le the concentration decays. The microorganisms plunge with the rise in Le and Lb, but it upsurges for Pe and σ.
- The local Nusselt number is enhancing w. r. t Pr for increasing Pr_m and it decays for θ_w alongside Rd, N_b and N_t respectively.
- The mass flux and local density number are decreasing along Pr_m and for diverse Le but the mass flux and local density number are increasing along N_t and for various N_b.
- The local density number is diminishing for Pe and σ along Lb and Pr_m respectively.

Nomenclature

$r,\ \theta^*, z$	Cylindrical coordinates	k^*	Mean absorption coefficient
u, v, w	Velocity components along $r,\ \theta^*$and z	σ	Bio-convection parameter
F, G, H	Dimensionless components of the velocity in radial, azimuthal, and axial directions.	D_B, D_T, D_N	Brownian diffusion, thermophoresis diffusion Coefficients, and microorganisms diffusivity
C	Concentration of nano-particles	N	The motile density of microorganisms
q_r	Radiative heat flux	Ω	Angular velocity
T_w, T_∞	Uniform surface temperature and ambient fluid temperature	$C_{Fr}, C_{G\theta^*}$	Radial and azimuthal directions skin friction coefficients

η	Dimensionless similarity variable	W_c	Maximum cell swimming speed of microorganisms
k	Thermal conductivity of power-law fluid	θ	Dimensionless temperature
M	Magnetic parameter	λ	Velocity ratio parameter
Nu_r	Local Nusselt number	σ^*	Stefan-Boltzmann constant
Re_r	Local Reynolds number	Pr	Prandtl number
u_e, v_e	Free stream velocities	θ_w	Temperature ratio parameter
B_0	Uniform magnetic field	ω	Rotation parameter
C_w, C_∞	Surface and ambient concentrations of nanoparticle	α_f	Thermal diffusivity
$(\rho c_p)_f$	Specific heat at constant pressure of the fluid	N_w, N_∞	Wall and ambient concentrations of microorganisms
T	Fluid temperature	$\tau_{rz}, \tau_{\theta^* z}$	Radial and azimuthal shear stresses
ν_f	Kinematic viscosity	ρ_f	Density of fluid
φ	The dimensionless concentration of nano-particles	S	The dimensionless density of motile microorganisms
n	Power-law index	τ	The ratio of the effective heat capacity
N_b	Brownian motion parameter	N_t	Thermophoresis parameter
Pr_m	Modified Prandtl number	Le	Lewis number
Lb	Bio-convection Lewis number	Pe	Peclet number
μ	Dynamic viscosity	Nn_r	Local motile density number of microorganisms
q_n	Surface motile microorganisms flux	k_f	Nano-particles thermal conductivity
q_w	Constant heat flux	q_m	Surface mas flux
Rd	Radiation parameter	μ_f	Nano-particles dynamic viscosity
σ_e	Effective electrical conductivity	b	Chemotaxis constant

Conflicts of Interest: The authors declare that they have no conflicts of interest to report regarding the present study.

References

[1] Von Kármán T 1921 Über laminare und turbulente reibung Zeitschrift für Angewandte Mathematik und Mechanik **1** 233–252.

[2] Cochran W G, Goldstein S 1934 The flow due to a rotating disc Math Proc Camb Philos Soc **30** 365-375.

[3] Sakiadis B C 1961 Boundary-layer behavior on continuous solid surfaces: I. Boundary-layer equations for two-dimensional and axisymmetric flow AICHE Journal **7** 26-28.

[4] Erickson L E, Fan L T and Fox V G 1966 Heat and mass transfer on moving continuous flat plate with suction or injection Ind Eng Chem Fund **5** 19–25.

[5] Crane L J 1970 Flow past a stretching plate Zeitschrift für angewandte Mathematik und Physik **21** 645-647.

[6] Rajagopal K R, Na T Y and Gupta A S 1984 Flow of a viscoelastic fluid over a stretching sheet Rheologica Acta **23** 213-215.

[7] Chen C H 2008 Effects of magnetic field and suction/injection on convection heat transfer of non-Newtonian power-law fluids past a power-law stretched sheet with surface heat flux International Journal of Thermal Sciences, **47** 954-961.

[8] Turkyilmazoglu M 2012 MHD fluid flow and heat transfer due to a stretching rotating disk Int J Therm Sci **51** 195–201.

[9] Srinivas S, Subramanyam Reddy A, Ramamohan T R and Shukla A K 2014 Thermal-diffusion and diffusion-thermo effects on MHD flow of viscous fluid between expanding or contracting rotating porous disks with viscous dissipation J Egypt Math Soc **1** 100–107.

[10] Hannah D M 1952 Forced Flow against a Rotating Disc. COWL London No. 2772 Rep Memor Aero Res worldcat.org/title/forced-flow-against-a-rotating-disc/oclc/30161905. Accesed1952.

[11] Wang C Y 2008 Off-centered stagnation flow towards a rotating disc Int J Eng Sci **46** 391–396.

[12] Irfan Mustafa, Tariq Javed and Abuzar Ghaffari 2016 Heat transfer in MHD stagnation point flow of a ferrofluid over a stretchable rotating disk Journal of Molecular Liquids **219** 526–532.

[13] Turkyilmazoglu M 2012 Three-dimensional MHD stagnation flow due to a stretchable rotating disk International Journal of Heat and Mass Transfer **55** 6959–6965.

[14] Shateyi S and Makinde O D 2013 Hydromagnetic stagnation-point flow towards a radially stretching convectively heated disk Mathematical Problems in Engineering **2013** 1-8.

[15] Freidoonimehr N, Rashidi MM, Mahmud S and Nazari F 2015 Slip effects on MHD stagnation point-flow and heat transfer over a porous rotating disk Physical Science International Journal **5** 34–50.

[16] Hayat T, Qayyum S, Waqas M and Ahmed B 2017 Influence of thermal radiation and chemical reaction in mixed convection stagnation point flow of Carreau fluid Results in Physics **7** 4058-4064.

[17] Hayat T, Qayyum S, Imtiaz M and Alsaedi A 2017 Homogeneous-heterogeneous reactions in nonlinear radiative flow of Jeffrey fluid between two stretchable rotating disks Results in Physics **7** 2557-2567.

[18] Tasawar Hayat, Uzma Shaheen, Anum Shafiq, Ahmed Alsaedi and Saleem Asghar 2015 Marangoni mixed convection flow with Joule heating and nonlinear radiation AIP Advances **5** 077140.

[19] Mitschka P 1964 Nicht-Newtonsche Flüssigkeiten II. Drehstromungen Ostwald-de Waelescher Nicht-Newtonscher Flüssigkeiten Collection of Czechoslovak Chemical Communications **29** 2892–2905.

[20] Mitschka P and Ulbricht J 1965 Nicht-Newtonsche Flüssigkeiten IV Strömung Nicht-Newtonscher Flüssigkeiten Ostwald-de Waeleschen Typs in der Umgebung Rotierender Drehkegel und Schieben Collection of Czechoslovak Chemical Communications **30** 2511-2526.

[21] Andersson H I, Korte E De and Meland E R 2001 Flow of a Power-Law Fluid over a Rotating Disk Revisited Fluid Dynamics Research **28** 75-88.

[22] Andersson H I and Korte E de 2002 MHD flow of a power-law fluid over a rotating disk European Journal of Mechanics B/Fluids **21** 317–324.

[23] Chunying Ming, Liancun Zheng, Xinxin Zhang 2011 Steady flow and heat transfer of the power-law fluid over a rotating disk International Communications in Heat and Mass Transfer **38** 280–284.

[24] Chunying Ming, Liancun Zheng, Xinxin Zhang and Liu F Anh V 2016 Flow and heat transfer of power-law fluid over a rotating disk with generalized diffusion International Communications in Heat and Mass Transfer **79** 81-88.

[25] Usman, Ping Lin and Abuzar Ghaffari 2020 Steady flow and heat transfer of the power-law fluid between two stretchable rotating disks with non-uniform heat source/sink Journal of Thermal Analysis and Calorimetry https://doi.org/10.1007/s10973-020-10142-x.

[26] Waleed Ahmad Khan M, Ijaz Khan M, Hayat T and Alsaedi A 2019 Numerical solution of MHD flow of power law fluid subject to convective boundary conditions and entropy generation Computer Methods and Programs in Biomedicine

https://doi.org/10.1016/j.cmpb.2019.105262.

[27] Choi S U S, 1995 Enhancing thermal conductivity of fluids with nanoparticles, Proc Int Mech Eng Congress San Francisco USA ASME FED 231/MD 66 99–105.

[28] Tiwari R J and Das M K 2007 Heat transfer augmentation in a two sided lid driven differentially heated square cavity utilizing nanofluids International Journal of Heat Mass Transfer **50** 2002–2018.

[29] Jawad Ahmed, Masood Khan and Latif Ahmad 2019 Stagnation point flow of Maxwell nanofluid over a permeable rotating disk with heat source/sink Journal of Molecular Liquids **287** 110853.

[30] Abdul Hafeez, Masood Khan and Jawad Ahmed 2020 Stagnation point flow of radiative Oldroyd-B nanofluid over a rotating disk Computer Methods and Programs in Biomedicine https://doi.org/10.1016/j.cmpb.2020.105342.

[31] Nilankush Acharya, Raju Bag and Prabir Kumar Kundu 2019 Influence of Hall current on radiative nanofluid flow over a spinning disk: A hybrid approach Physica E: Low-dimensional Systems and Nanostructures **111** 103–112.

[32] Hayat T, Rashid M, Khan MI and Alsaedi A 2018 Melting heat transfer and induced magnetic field effects on flow of water based nanofluid over a rotating disk with variable thickness Results in Physics **9** 1618–1630.

[33] Kuznetsov A V 2005 Thermo-bioconvection in a suspension of oxytactic bacteria Int Commun Heat Mass Transfer **32** 991–999.

[34] Kuznetsov A V 2005 The onset of bioconvection in a suspension of negatively geotactic microorganisms with high frequency vertical vibration Int Commun Heat Mass Transfer **32** 1119–1127.

[35] Kuznetsov A V 2011 Nanofluid bioconvection in water-based suspensions containing nanoparticles and oxytactic microorganisms: oscillatory instability Nanoscale Res Lett **6** 1–13.

[36] Kuznetsov A V 2010 The onset of nanofluid bioconvection in a suspension containing both nanoparticles and gyrotactic microorganisms Int Commun Heat Mass Transfer **37** 1421–1425.

[37] Hui Chen, Jiayang Chen, Yao Geng and Kai Chen 2017 Three-dimensional boundary layer flow over a rotating disk with power-law stretching in a nanofluid containing gyrotactic microorganisms Heat Transfer—Asian Res **2017** 1–14.

[38] Ferdows M, Gnaneswara Reddy M, Shuyu Sun and Faris Alzahrani 2019 Two-dimensional gyrotactic microorganisms flow of hydromagnetic power law nanofluid past an elongated sheet Advances in Mechanical Engineering **11** 1-17.

[39] Muhammad Mubashir Bhatti, Anwar Shahid, Tehseen Abbas, Sultan Z Alamri and Rahmat Ellahi 2020 Study of Activation Energy on the Movement of Gyrotactic Microorganism in a Magnetized Nanofluids Past a Porous Plate Processes https://doi.org/10.3390/pr8030328.

[40] Mohamed Abd El-Aziz and Aly AM 2020 MHD Boundary Layer Flow of a Power-Law Nanofluid Containing Gyrotactic Microorganisms Over an Exponentially Stretching Surface Computers, Materials & Continua **62** 525-549.

[41] Dulal Pal and Surya Kanta Mondal 2019 Magneto-bioconvection of Powell Eyring nanofluid over a permeable vertical stretching sheet due to gyrotactic microorganisms in the presence of nonlinear thermal radiation and Joule heating International Journal of Ambient Energy https://doi.org/10.1080/01430750.2019.1679253.

[42] Salma Zaman and Mahwish Gul 2019 Magnetohydrodynamic bioconvective flow of Williamson nanofluid containing gyrotactic microorganisms subjected to thermal radiation and Newtonian conditions Journal of Theoretical Biology **479** 22-28.

[43] Ijaz Khan M, Fazal Haq, Sohail A Khan, Hayat T and Imran Khan M 2019 Development of thixotropic nanomaterial in fluid flow with gyrotactic microorganisms, activation energy, mixed convection Computer Methods and Programs in

Biomedicine https://doi.org/10.1016/j.cmpb.2019.105186.

[44] Rahila Naz, Sana Tariq and Hamed Alsulami 2020 Inquiry of entropy generation in stratified Walters' B nanofluid with swimming gyrotactic microorganisms Alexandria Eng J https://doi.org/10.1016/j.aej.2019.12.037.

[45] Alzahrani E O, Shah Z, Dawar A and Malebary S J 2019 Hydromagnetic mixed convective third grade nanomaterial containing gyrotactic microorganisms toward a horizontal stretched surface Alexandria Engineering Journal **58** 1421-1429.

[46] Naz R, Noor M, Hayat T, Javed M and Alsaedi A 2020 Dynamism of magnetohydrodynamic cross nanofluid with particulars of entropy generation and gyrotactic motile microorganisms International Communications in Heat and Mass Transfer https://doi.org/10.1016/j.icheatmasstransfer.**2019**.104431.

[47] Waqas H, Khan SU, Hassan M, Bhatti MM and Imran M 2019 Analysis on the bioconvection flow of modified second-grade nanofluid containing gyrotactic microorganisms and nanoparticles Journal of Molecular Liquids https://doi.org/10.1016/j.molliq.2019.111231.

[48] Mehryan S A M, Moradi Kashkooli F, Soltani M and Raahemifar K 2016 Fluid Flow and Heat Transfer Analysis of a Nanofluid Containing Motile Gyrotactic Micro-Organisms Passing a Nonlinear Stretching Vertical Sheet in the Presence of a Non- Uniform Magnetic Field; Numerical Approach PLOS ONE https://doi.org/10.1371/journal. pone.0157598.

[49] Khan W A and Pop I 2010 Boundary-layer flow of a nanofluid past a stretching sheet Int J Heat Mass Transf **53** 2477–2483.

[50] Oyelakin I S et al 2019 Bioconvection in Casson nanofluid flow with Gyrotactic microorganisms and variable surface heat flux International Journal of Biomathematics https://doi.org/10.1142/S1793524519500414.